atoms

MDPI

Article

Magic Wavelengths for *1S–nS* and *2S–nS* Transitions in Hydrogenlike Systems

Chandra M. Adhikari [1,*], Jonathan C. Canales [1,2], Thusitha P. W. Arthanayaka [2] and Ulrich D. Jentschura [3]

1 Department of Chemistry, Physics and Materials Science, Fayetteville State University, Fayetteville, NC 28301, USA; jcanales@skidmore.edu
2 Department of Physics, Skidmore College, Saratoga Springs, NY 12866, USA; twkulati@skidmore.edu
3 Department of Physics, Missouri University of Science and Technology, Rolla, MO 65409, USA; ulj@mst.edu
* Correspondence: cadhikari@uncfsu.edu

Abstract: We study the magic wavelength for two-photon 1*S*–*nS* transitions in a hydrogen and deuterium atom, as well as 2*S*–*nS* transitions, where the lower level is the metastable 2*S* state. At the magic wavelength, the dynamic Stark shifts of the ground and the excited state of the transition coincide, so that the transition frequency is independent of the intensity of the trapping laser field. Experimentally feasible magic wavelengths of transitions with small slopes in the atomic polarizabilities are determined; these are the most stable magic wavelengths against variations of the laser frequency. We provide data for the magic wavelengths for the 1*S*–*nS* and 2*S*–*nS* transitions in hydrogen and deuterium, with $n = 2, \ldots, 8$. We also analyze the stability of the elimination of the ac Stark shift at the magic wavelength against tiny variations of the trapping laser frequency from the magic value.

Keywords: magic wavelength; polarizabilities; atomic transitions; optical trapping

PACS: 11.15.Bt; 11.10.Jj

check for updates

Citation: Adhikari, C.M.; Canales, J.C.; Arthanayaka, T.P.W.; Jentschura, U.D. Magic Wavelengths for *1S–nS* and *2S–nS* Transitions in Hydrogenlike Systems. *Atoms* **2022**, *10*, 1. https://doi.org/10.3390/atoms10010001

Academic Editor: G. W. F. Drake

Received: 23 November 2021
Accepted: 16 December 2021
Published: 22 December 2021

1. Introduction

Optical lattice-clocks and optical dipole traps are at the forefront of modern scientific research in ultracold atoms [1–4]. An oscillating (ac) electric field plays a vital role in trapping an atom by a laser. However, the ac Stark shift introduced by the trapping laser field constitutes an obstacle, because the frequency of the transition whose frequency is to be measured, gets shifted significantly by the trapping light field [5,6]. For a specific atomic reference state $|\phi\rangle$, the ac Stark shift is given as [7]:

$$\Delta E_{\rm ac}(\phi, \omega_L) = -\frac{I_L}{2\epsilon_0 c}\,\alpha(\phi, \omega_L)\,, \tag{1}$$

where I_L is the laser intensity, ϵ_0 is the permittivity of free space, c is the speed of light in a vacuum, and $\alpha(\phi, \omega_L)$ is the dynamic polarizability of the atomic state $|\phi\rangle$ as a function of the angular frequency ω_L of the incident (trapping) laser. The dynamic polarizability is generally different for the ground state of an atom in comparison to its excited states. There are, however, some distinct, so-called magic laser wavelengths, where the ac Stark shifts of the two atomic states involved in a transition become equal to each other. At a magic wavelength, the ac Stark shift does not alter the transition frequency as it cancels in the difference of the shifts of the ground and excited states [4,8–12].

This work concentrates on the 1*S*–*nS* and 2*S*–*nS* transitions in hydrogen and deuterium. Transitions between different hydrogen and deuterium energy levels, their comparison with hydrogen, and the study of the isotope effect represent topics of fundamental interest in atomic physics and precision measurements [13–17].

The International System of Units (SI), sometimes referred to as the SI mksA unit system, is used throughout the paper (base units are meter, second, kilogram, and Ampere). We organize this paper as follows: In Section 2, we first evaluate a few matrix elements useful in the calculation of the dynamic polarizability (see Refs. [18–30]). At first, angular components of the matrix elements are calculated as presented in Ref. [31], and then the radial components are evaluated. The evaluation of the radial components is done using the Sturmian decomposition of the Schrödinger Green function [19–21], and then the radial integrations are done. We take into account the summations over the discrete and continuous spectra. The continuum states significantly contribute to the Stark shift for the ground state of hydrogen [28,32]. In Section 3, magic wavelengths for $1S$–nS and $2S$–nS transitions are calculated for hydrogen and deuterium. In Section 4, we discuss the leading reduced-mass and other corrections to the magic wavelengths. Finally, conclusions are drawn in Section 5.

2. Dynamic Polarizability of *nS* States

We consider the following matrix element of the Schrödinger–Coulomb propagator [23,33,34] of the hydrogen atom, for a reference state $|\phi_n\rangle$,

$$P(\phi_n;\omega_L) = \frac{e^2}{3}\left\langle \phi_n \middle| \vec{r}\left(\frac{1}{H_s - E_n + \hbar\omega_L}\right)\vec{r} \middle| \phi_n \right\rangle, \tag{2}$$

where $\vec{r}$ is the electron position operator, and $H_s = \vec{p}^{\,2}/(2\mu) - e^2/(4\pi\epsilon_0 r)$ is the atomic Schrödinger Hamiltonian. The bound-state energy is $E_n = -(\alpha^2\mu c^2)/(2n^2)$. The momentum operator is denoted as $\vec{p}$, and the reduced mass of the system is μ. Furthermore, E_n is the energy, and, in the context of the current investigation, ω_L is the angular frequency of the (trapping-field) laser. We use the well-known expression for the Schrödinger–Coulomb bound state $\Psi_{n\ell m}(\vec{r}) = \Psi_{n\ell m}(r,\theta,\varphi) = R_{n\ell}(r)\, Y_{\ell m}(\theta,\varphi)$ in the coordinate representation,

$$R_{n\ell}(r) = \left[\frac{(n-\ell-1)!}{(n+\ell)!}\right]^{1/2} \frac{2^{\ell+1}}{n^2}\frac{1}{\mathrm{a}_0^{3/2}}\left(\frac{r}{n\,\mathrm{a}_0}\right)^{\ell} \exp\left(-\frac{r}{n\,\mathrm{a}_0}\right) L_{n-\ell-1}^{2\ell+1}\left(\frac{2r}{n\mathrm{a}_0}\right). \tag{3}$$

Here,

$$\mathrm{a}_0 = \frac{\hbar}{\alpha\mu c} \tag{4}$$

is a generalized Bohr radius, adapted to the reduced mass of the system. The spherical harmonic of the angular part is $Y_{\ell m}(\theta,\varphi)$,

$$Y_{\ell m}(\theta,\varphi) = \left[\frac{(2\ell+1)(\ell-m)!}{4\pi(\ell+m)!}\right]^{1/2} P_\ell^m(\cos(\theta))\,\mathrm{e}^{\mathrm{i}m\varphi}. \tag{5}$$

Here, $L_n^\ell(x)$ is the associated Laguerre polynomial, and $P_\ell^m(\cos(\theta))$ is the associated Legendre polynomial. Also, n, ℓ and m are the principal, orbital angular and magnetic orbital quantum numbers, respectively. The Green function $G(\vec{r}_1,\vec{r}_2,\omega_L)$ of the Schrödinger–Coulomb Hamiltonian H_s fulfills the second-order differential equation:

$$(H_s - E_n + \hbar\omega_L)\, G(\vec{r}_1,\vec{r}_2,\omega_L) = \delta^{(3)}(\vec{r}_1 - \vec{r}_2) \tag{6}$$

and can be expressed in terms of radial Green function $g_\ell(r_1,r_2,\nu_n)$, and spherical harmonics $Y_{\ell m}(\theta_i,\varphi_i)$ as [19]:

$$G(\vec{r}_1,\vec{r}_2,\nu_n) = \sum_{\ell=0}^{\infty}\sum_{m=-\ell}^{\ell} g_\ell(r_1,r_2,\nu_n)\; Y_{\ell m}(\theta_1,\varphi_1)\; Y^*_{\ell m}(\theta_2,\varphi_2). \tag{7}$$

It is convenient to define the dimensionless energy variable $t_n = t_n(\omega_L)$, which parameterizes the laser frequency,

$$t_n \equiv t_n(\omega_L) = \left(1 + \frac{2\,n^2\,\hbar\omega_L}{\alpha^2 \mu c^2}\right)^{-1/2}, \qquad [n\,t_n(\omega_L)]^2 = -\frac{\alpha^2\,\mu\,c^2}{2(E_n - \omega_L)}\,. \tag{8}$$

The quantity ν_n acts as a generalization of the principal quantum number n of the reference state, to non-integer ν_n, as follows,

$$\nu_n \equiv \nu_n(\omega_L) = n\,t_n = n\,t_n(\omega_L)\,. \tag{9}$$

The low-frequency limits are $\nu_n \to n$ and $t_n \to 1$ for $\omega_L \to 0$, and the high-frequency limit is $t_n \to 0$ for $\omega_L \to \infty$. The fine-structure constant is denoted as α, and c is the speed of light. In the so-called Sturmian form, the radial Green function $g_\ell(r_1, r_2, \omega_L)$ can be written as [19–21]:

$$\begin{aligned} g_\ell(r_1, r_2, \omega_L) &= \frac{2\mu}{\hbar^2}\left(\frac{2}{\mathrm{a}_0 \nu_n}\right)^{2\ell+1} (r_1 r_2)^\ell \, \exp\left(-\frac{r_1 + r_2}{\mathrm{a}_0 \nu_n}\right) \\ &\quad \times \sum_{k=0}^{\infty} \frac{k!\; L_k^{2\ell+1}\left(\frac{2r_1}{\mathrm{a}_0\nu_n}\right)\; L_k^{2\ell+1}\left(\frac{2r_2}{\mathrm{a}_0\nu_n}\right)}{(k+2\ell+1)!\;\;(k+\ell+1-\nu_n)}\,, \end{aligned} \tag{10}$$

where $\nu_n \equiv \nu_n(\omega_L)$. If the reference states is an nS state with $\ell = 0$, then one can express Equation (2) in integral form,

$$P(\phi_n; \omega_L) = \frac{e^2}{3} \int_0^\infty \mathrm{d}r_1\, r_1^3 \int_0^\infty \mathrm{d}r_2\, r_2^3\, R_{n0}(r_1)\, g_{\ell=1}(r_1, r_2, \nu_n = n t_n)\, R_{n0}(r_2)\,, \tag{11}$$

where t_n is defined in Equation (8). For a ground state hydrogen ($n = 1$), for example, the radial part of the wave function reads $R_{10}(r) = 2\,\mathrm{a}_0^{-3/2}\,\exp(-r/\mathrm{a}_0)$. Substituting the radial part $R_{10}(r)$ and using the Sturmian form of the radial Green function from Equation (10) in Equation (11), one obtains:

$$\begin{aligned} P(1S; \omega_L) &= \frac{64\,\mu\,e^2}{3\hbar^2\,\mathrm{a}_0^6\,t_1^3} \int_0^\infty r_1^4\,\mathrm{d}r_1 \int_0^\infty r_2^4\,\mathrm{d}r_2\, \exp\left(-\frac{r_1 + r_2}{\mathrm{a}_0 t_1}\right) \\ &\quad \times \exp\left(-\frac{r_1 + r_2}{\mathrm{a}_0}\right) \sum_{k=0}^{\infty} \frac{k!\; L_k^3\left(\frac{2r_1}{\mathrm{a}_0 t_1}\right) L_k^3\left(\frac{2r_2}{\mathrm{a}_0 t_1}\right)}{(k+3)!\,(k+2-t_1)}\,, \end{aligned} \tag{12}$$

which after some algebra works out to [9,24,25,28,29]:

$$\begin{aligned} P(1S; \omega_L) &= \frac{\hbar^2 e^2}{\alpha^4 \mu^3 c^4}\left[\frac{2\,t_1^2(-3 + 3t_1 + 12t_1^2 - 12t_1^3 - 19t_1^4 + 19t_1^5 + 26t_1^6 + 38t_1^7)}{3(-1+t_1)^5\,(1+t_1)^4}\right. \\ &\quad \left. - \frac{256\,t_1^9}{3(-1+t_1)^5(1+t_1)^5}\; {}_2F_1\left(1, -t_1; 1 - t_1; \left(\frac{1-t_1}{1+t_1}\right)^2\right)\right]. \end{aligned} \tag{13}$$

We take the opportunity to correct a sign error in the term multiplying the hypergeometric function in Equation (3a) of Ref. [9]. In the static limit $t_1 \to 1$ ($\omega_L \to 0$), Equation (13) yields half the the static polarizability,

$$P(1S; \omega_L \to 0) = \frac{9e^2\hbar^2}{4\alpha^4\mu^3c^4} + \mathcal{O}(\omega_L^2)\,. \tag{14}$$

For $t_1 \to 0$ ($\omega_L \to \infty$), the leading asymptotic terms are:

$$P(1S;\omega_L \to \infty) = \frac{3\,\hbar^2 e^2}{\alpha^2 \mu^2 c^2}\frac{1}{\hbar\omega_L} - \frac{3\hbar^2 e^2}{2\mu}\frac{1}{\hbar^2\omega_L^2} + \mathcal{O}(\omega_L^{-3})\,. \tag{15}$$

Following the same procedure for $2S$ and $3S$ states, one obtains [9,25,28,29]:

$$\begin{aligned} P(2S;\omega_L) = \frac{\hbar^2 e^2}{\alpha^4\mu^3 c^4}\Bigg[& \frac{16 t_2^2}{3(t_2-1)^6(t_2+1)^4}\Big(1181 t_2^8 - 314 t_2^7 - 16 t_2^6 - 166 t_2^5 + 14 t_2^4 + 138 t_2^3 \\ & -48 t_2^2 - 42 t_2 + 21\Big) - \frac{16384 t_2^9 (4t_2^2-1)}{3\left(t_2^2-1\right)^6}\, {}_2F_1\left(1,-2t_2;1-2t_2;\frac{(1-t_2)^2}{(1+t_2)^2}\right)\Bigg], \end{aligned} \tag{16}$$

for the $2S$ state. For the $3S$ state, one has the result:

$$\begin{aligned} P_{3S}(\omega_L) = \frac{\hbar^2 e^2}{\alpha^4\mu^3 c^4}\Bigg[& \frac{54 t_3^2}{(t_3-1)^8(t_3+1)^6}\Big(15538 t_3^{12} - 2852 t_3^{11} - 13283 t_3^{10} + 2090 t_3^9 \\ & +2871 t_3^8 + 40 t_3^7 - 62 t_3^6 - 492 t_3^5 + 128 t_3^4 + 236 t_3^3 - 95 t_3^2 - 46 t_3 + 23\Big) \\ & - \frac{6912 t_3^9 \left(7t_3^2-3\right)^2 (9t_3^2-1)}{\left(t_3^2-1\right)^8}\, {}_2F_1\left(1,-3t_3;1-3t_3;\frac{(1-t_3)^2}{(1+t_3)^2}\right)\Bigg]. \end{aligned} \tag{17}$$

The dynamical polarizability $\alpha_{\phi_n}(\omega_L)$ for a reference state ϕ_n is the sum:

$$\alpha(\phi_n;\omega_L) = P(\phi_n;\omega_L) + P(\phi_n;-\omega_L)\,. \tag{18}$$

As a check, in the static limit, we have $\alpha(\phi_n;\omega_L \to 0) = 2P(\phi_n;\omega_L \to 0)$, so that the well-known static polarizability of the ground state:

$$\alpha(1S;\omega_L \to 0) = \frac{9\,e^2\hbar^2}{2\alpha^4\mu^3 c^4} \tag{19}$$

is confirmed. The above formalism is adapted to take into account the reduced mass of the system, which is different for hydrogen as opposed to deuterium. If one were to carry out the calculation with the reduced mass μ of the system being replaced by the electron mass m_e, then the appropriate scaling factor for the magic angular frequency is μ/m_e, where m_e is the electron mass. The polarizability itself contains two matrix elements of the position operator, which each scale with the factor m_e/μ, while the propagator denominator scales with μ/m_e, resulting in a total scaling factor $(m_e/\mu)^3$ for the polarizability.

3. Magic Wavelength

Whenever the wavelength of an incident laser matches its magic value, the ac Stark shifts of the ground and excited states of a transition become identical. For example, in the transition $\phi_i \to \phi_f$ (initial to final states), we have according to Equation (1),

$$\Delta E_{\rm ac}(\phi_i;\omega_L = \omega_M) = \Delta E_{\rm ac}(\phi_f;\omega_L = \omega_M)\,, \tag{20}$$

where the magic angular frequency ω_M and the the magic frequency ν_M are given by:

$$\omega_M = 2\pi c/\lambda_M\,, \qquad \nu_M = c/\lambda_M\,, \tag{21}$$

respectively. In addition, λ_M is the magic laser wavelength. In the following, we will use the terms of magic wavelength and magic frequency interchangeably, with the conversion being understood according to Equation (21). For a chosen laser intensity, the ac Stark shift of two levels depends on the polarizabilities of two atomic states. Thus, the magic wavelength λ_M of the $1S$–nS transition can be determined by the condition:

$$\alpha_\Delta(\lambda_M) \equiv \alpha(\phi_f;\omega_M) - \alpha(\phi_i;\omega_M) = 0\,, \quad (22)$$

where $|\phi_f\rangle = |nS\rangle$, and $|\phi_i\rangle = |1S\rangle$ or $|2S\rangle$. The quantity $\nu_M = c/\lambda_M = \omega_M/(2\pi)$ gives the magic frequency in Hz (see also Tables 1 and 2).

Table 1. The most stable magic wavelengths and slopes at that magic wavelengths for $1S$–nS and $2S$–nS transitions for hydrogen.

Transition	ν_M [10^{14} Hz]	λ_M [nm]	ζ [Hz $\left(\frac{\mathrm{cm}^2}{\mathrm{kW}}\right)$]	ξ [$\frac{\mathrm{Hz}}{\mathrm{GHz}}\left(\frac{\mathrm{cm}^2}{\mathrm{kW}}\right)$]	χ [$\frac{e^2\,a_0^2/E_h}{\mathrm{nm}}$]
$1S$–$2S$	5.82521	514.646	−221.58	−1.3563	−5.2186
$1S$–$3S$	2.18531	1371.85	−212.65	−20.192	−10.934
$1S$–$4S$	1.06583	2812.77	−211.59	−179.26	−23.089
$1S$–$5S$	0.60703	4938.67	−211.37	−1271.8	−53.138
$1S$–$6S$ (I)	0.47495	6312.10	−211.33	−1058.6	−27.077
$1S$–$6S$ (II)	0.42254	7094.95	−211.32	+2445.1	+49.501
$1S$–$7S$	0.32391	9255.47	−211.30	−5859.6	−69.707
$1S$–$8S$	0.22944	13,066.4	−211.28	−18966.	−113.21
$2S$–$3S$	2.20479	1359.73	−7063.5	−24.202	−13.340
$2S$–$4S$	1.06779	2807.60	−5909.3	−185.94	−24.039
$2S$–$5S$	0.60730	4936.47	−5719.7	−1287.3	−53.831
$2S$–$6S$ (I)	0.47527	6307.82	−5686.1	−1077.7	−27.603
$2S$–$6S$ (II)	0.42241	7097.28	−5675.0	+2494.1	+50.459
$2S$–$7S$	0.32397	9253.80	−5657.9	−5887.3	−70.062
$2S$–$8S$	0.22946	13,065.4	−5645.9	−19,007	−113.47

Table 2. The most stable magic wavelengths and slopes at that magic wavelengths for $1S$–nS and $2S$–nS transitions for deuterium.

Transition	ν_M [10^{14} Hz]	λ_M [nm]	ζ [Hz $\left(\frac{\mathrm{cm}^2}{\mathrm{kW}}\right)$]	ξ [$\frac{\mathrm{Hz}}{\mathrm{GHz}}\left(\frac{\mathrm{cm}^2}{\mathrm{kW}}\right)$]	χ [$\frac{e^2\,a_0^2/E_h}{\mathrm{nm}}$]
$1S$–$2S$	5.82680	514.506	−221.40	−1.3549	−5.2129
$1S$–$3S$	2.18590	1371.48	−212.48	−20.171	−10.922
$1S$–$4S$	1.06612	2812.00	−211.42	−179.06	−23.065
$1S$–$5S$	0.60720	4937.32	−211.20	−1270.4	−53.080
$1S$–$6S$ (I)	0.47508	6310.38	−211.16	−1057.5	−27.048
$1S$–$6S$ (II)	0.42266	7093.02	−211.15	+2442.5	+49.447
$1S$–$7S$	0.32400	9252.95	−211.12	−5853.2	−69.631
$1S$–$8S$	0.22950	13,062.9	−211.11	−18946.	−113.08
$2S$–$3S$	2.20539	1359.36	−7057.7	−24.175	−13.325
$2S$–$4S$	1.06808	2806.84	−5904.5	−185.74	−24.013
$2S$–$5S$	0.60747	4935.12	−5715.1	−1285.9	−53.773
$2S$–$6S$ (I)	0.47540	6306.11	−5681.4	−1076.5	−27.573
$2S$–$6S$ (II)	0.42252	7095.35	−5670.4	+2491.4	+50.404
$2S$–$7S$	0.32406	9251.28	−5653.3	−5880.9	−69.985
$2S$–$8S$	0.22952	13,061.8	−5641.2	−18,986.	−113.34

The polarizabilities of the ground state and the $2S$ and $3S$ excited states of hydrogen, as a function of the laser wavelength, are shown in Figure 1. The polarizabilities are expressed in atomic units, i.e., in units of $e^2\,a_0^2/E_h$. Wavelengths are presented in nanometers. Images (a) and (b) of Figure 1 present a general picture of the dynamic polarizabilities with the magic frequencies indicated. Images (b) and (d) of Figure 1 show the polarizabilities near their intersections, i.e., near the magic wavelength. Note that the polarizabilities of the excited states vary over many orders of magnitude over the range of investigated frequencies and becomes singular at resonances, while the ground-state polarizability remains of the same order-of-magnitude as the static value as discussed in Equations (14), (18) and (19).

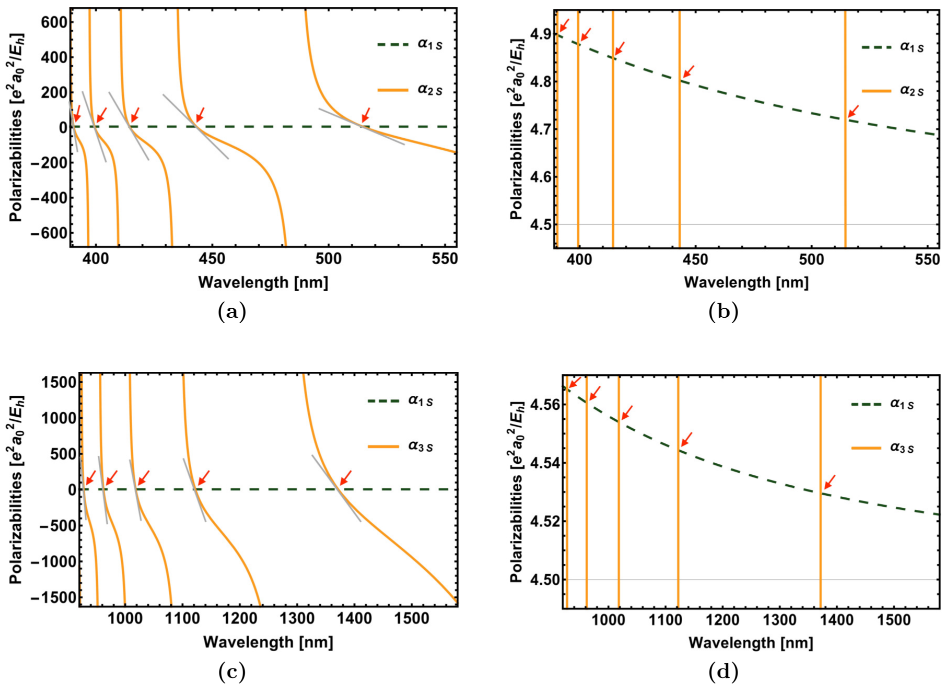

Figure 1. We investigate the polarizabilities of $1S$ and $2S$ states of hydrogen as a function of incident wavelength of the incident laser (**a**) and the same for $1S$ and $3S$ states of hydrogen (**c**). Polarizabilities near the points of intersections are shown in (**b**,**d**), with the scale of the ordinate axis decreased. Polarizabilities are expressed in atomic units, i.e., in units of $e^2 a_0^2/E_h$, where $a_0 = \hbar/(\alpha m_e c)$ is the Bohr radius (not adapted to the reduced mass of the system). We recall that the Bohr radius, adapted to the reduced mass, is $\mathrm{a}_0 = \hbar/(\alpha\mu c)$ (see Equation (4)). Also, m_e is the electron mass, and c is the speed of light. The Hartree energy is $E_h = \alpha^2 m_e c^2$. The wavelengths corresponding to the points of intersection are the magic wavelengths.

For reference, in Tables 1 and 2, we also give the ac Stark shifts, converted to frequency units, of each individual level at the magic wavelength, normalized to the incident trapping laser intensity,

$$\zeta = \frac{1}{h}\frac{1}{I_L}\,\Delta E_{\rm ac}(\phi_f,\omega_M) = \frac{1}{h}\frac{1}{I_L}\,\Delta E_{\rm ac}(\phi_i,\omega_M)\,. \tag{23}$$

It is essential to ensure the stability of the resonance frequency against small deviations of the trapping laser field from the magic wavelength. The deviation of the ac Stark shift from the zero value attained at the magic wavelength, due to a slight variation of the trapping laser frequency from the magic value, is given as:

$$\xi = \frac{1}{h}\frac{1}{I_L}\,2\pi\,\frac{\partial}{\partial\omega_L}\big(\Delta E_{\rm ac}(\phi_f,\omega_L) - \Delta E_{\rm ac}(\phi_i,\omega_L)\big)\Big|_{\omega_L=\omega_M} \tag{24}$$

where we refer to Equation (1). The prefactor $1/I_L$ divides out the intensity of the trapping laser, while the other prefactor $1/h$ converts the result to frequency units. Finally, the prefactor 2π converts the derivative with respect to the angular frequency to a derivative with respect to the trapping laser frequency. Our quantity ξ defined in Equation (24) differs from the quantity η defined in Equation (9) of Ref. [9] by a factor 2π. We also take the opportunity to point out that the factor $1/I_L$ was inadvertently omitted from the expression in the middle of Equation (9) of Ref. [9] but is present in the final numerical value presented in Ref. [9]. The unit of ξ is the ac Stark shift, measured in Hz, divided by the deviation of the laser frequency from the magic value, measured in GHz, and the intensity of the exciting laser, measured in $\mathrm{kW/cm^2}$. The unit of ξ is thus $\mathrm{Hz/(GHz\,kW/cm^2)}$.

An alternative method of measuring the deviation is by calculating the change in the polarizability α_Δ, defined in Equation (22), against variations around the magic wavelength. For convenience, one can divide by the atomic unit of polarizability, which is $e^2 a_0^2/E_h$, where E_h is the Hartree energy. Then,

$$\chi = \frac{E_h}{e^2 a_0^2} \left\{ \frac{\partial \alpha_\Delta(\omega_L)}{\partial \omega_L} \bigg|_{\omega_L=\omega_M} \right\} \frac{\partial \omega_M}{\partial \lambda_M} = \frac{E_h}{e^2 a_0^2} \left\{ \frac{\partial \alpha_\Delta(\omega_L)}{\partial \omega_L} \bigg|_{\omega_L=\omega_M} \right\} \left(-\frac{2\pi c}{\lambda_M^2} \right). \tag{25}$$

The unit of χ is thus the inverse nanometer, because a dimensionless quantity is differentiated with respect to a wavelength.

According to the intersection points indicated with arrows in Figure 1a, some magic wavelengths for the $2S$–$1S$ transition are close to 514 nm, 443 nm, 414 nm, 399 nm, and 390 nm. One desires a magic wavelength, in which the polarizability has the minimum slope [9]. The polarizability has the minimum slope for the magic wavelength value near 514 nm. Hence it is the most stable one against small deviations of the laser frequency from the magic value (see also Tables 1 and 2). The wavelength 514 nm lies in between the $2S$–$3P$ hydrogen transition of 656.275 nm and the $2S$–$4P$ transition of 486.132 nm [13,14,35]. This indicates that there is no loss of atoms due to resonant driving. For the $1S$–$3S$ transition in hydrogen, some magic wavelengths are near 1371 nm, 1122 nm, 1018 nm, 961 nm, and 927 nm (see the intersection points indicated with arrows in Figure 1c). The 12-$3S$ hydrogen polarizability difference has the minimum slope value for the 1371.85 nm wavelength, and hence it is the most stable one. Wavelength 1371.85 nm lies in between the $3S$–$4P$ hydrogen transition of 1875.07 nm and the $3S$–$5P$ hydrogen transition of 1281.80 nm [13,14,35], indicating that there is no loss of atoms due to resonant driving. For the $1S$–$6S$ and $2S$–$6S$ transitions, we indicate two alternative magic wavelengths, with commensurate stability coefficients ξ and χ. The smallest magic frequency, for $1S$–$6S$ and $2S$–$6S$, has a somewhat worse stability against deviations frequency instabilities of the trapping laser.

The most stable magic wavelengths and slopes for a various $1S$–nS and $2S$–nS hydrogen and deuterium transitions are listed in Tables 1 and 2. The magic wavelengths in deuterium are almost the same but slightly smaller than the reduced-mass-corrected value in the analogous transitions in hydrogen. This is because the reduced mass of deuterium is slightly larger than the reduced mass of hydrogen.

4. Relativistic and Field–Configuration Corrections to Magic Wavelengths

A discussion on the accuracy of the result we have obtained is in order. One of the most important corrections comes from the reduced mass of the system, which is in the order of 10^{-3}; this correction is taken into account by the reduced-mass adapted treatment outlined in Section 2. Another important correction is of a relativistic origin. In order to account the relativistic corrections, one should make the following substitution [23] in the $\vec{r}$-matrix element of the polarizability as:

$$\left\langle \phi_n \middle| \vec{r} \left(\frac{1}{H_s - E_n + \hbar\omega_L} \right) \vec{r} \middle| \phi_n \right\rangle \to \left\langle \phi_n + \delta\phi_n \middle| \vec{r} \left(\frac{1}{H_s + \delta H - E_n - \delta E_n + \hbar\omega_L} \right) \vec{r} \middle| \phi_n + \delta\phi_n \right\rangle, \tag{26}$$

where δH is the relativistic Hamiltonian correction to the Schrödinger Hamiltonian H_s, and δE_n is the corresponding relativistic energy correction. Furthermore, $|\delta\phi_n\rangle$ is the relativistic wave function correction. All of these corrections have been discussed in the context of Lamb shift calculations [23]. The relativistic correction is of relative order $\alpha^2 \sim 10^{-4}$

and thus suppressed in comparison to the reduced-mass correction [36,37]. The dynamic polarizability and, hence, the magic wavelength also receive field-configuration dependent corrections [5], which depend on the exact position of the atom in the laser field (e.g., whether it is located at a minimum or maximum of the oscillating laser electric field). The field-configuration dependent corrections are also of the order of $\alpha^2 \sim 10^{-4}$ [5]. We refrain from a discussion of these effects because the mentioned corrections are not expected to limit experimental precision, in view of the relatively small slopes of the dynamic polarizabilities near the magic wavelengths, as given by the quantities ξ and χ given in Tables 1 and 2. The same applies to the hyperpolarizabilities, which give contributions to the fourth-order ac Stark shift [38].

5. Conclusions

We studied the magic wavelengths for the $1S$–nS and $2S$–nS transitions of hydrogen and deuterium. We determined the magic wavelengths in these transitions by calculating the polarizabilities of the atomic states of interest and then finding wavelengths at which the polarizabilities of the respective states cancel in the difference. The polarizabilities are provided by the nS states $\vec{r}$-matrix elements of the Schrödinger–Coulomb propagator, as discussed in Section 2. Following the determination of the magic wavelengths and corresponding trapping laser frequencies, we calculated the slopes of the dynamic Stark shifts with respect to the frequency of the trapping laser and summarized our results in Tables 1 and 2. We find that the stability of the elimination of the ac Stark shift against tiny deviations of the trapping laser frequency from the magic value decreases with the increasing quantum number of the excited final state of the transition.

Author Contributions: Conceptualization, C.M.A. and U.D.J.; software, all authors; investigation, all authors; writing—original draft preparation, all authors; writing—review and editing, C.M.A. and U.D.J. All authors have read and agreed to the published version of the manuscript.

Funding: This research was funded by the National Science Foundation (Grant PHY–2110294).

Institutional Review Board Statement: Not applicable.

Informed Consent Statement: Not applicable.

Data Availability Statement: All numerical data obtained as a result of the sutdies are contained in the manuscript.

Acknowledgments: The authors acknowledge helpful conversations with István Nándori and Krzysztof Pachucki. This research has been supported by the National Science Foundation (grant PHY–2110294).

Conflicts of Interest: The authors declare no conflict of interest.

References

1. Bloch, I. Ultracold quantum gases in optical lattices. *Nat. Phys.* **2005**, *1*, 23–30. [CrossRef]
2. Grimm, R.; Weidemüller, M.; Ovchinnikov, Y.B. Optical Dipole Traps for Neutral Atoms. *Adv. At. Mol. Opt. Phys.* **2000**, *42*, 95–170.
3. Nicholson, T.L.; Campbell, S.L.; Hutson, R.B.; Marti, G.E.; Bloom, B.J.; McNally, R.L.; Zhang, W.; Barrett, M.D.; Safronova, M.S.; Strouse, G.F.; et al. Systematic evaluation of an atomic clock at 2×10^{-18} total uncertainty. *Nat. Commun.* **2015**, *6*, 6896. [CrossRef]
4. Katori, H.; Takamoto, M.; Pal'chikov, V.G.; Ovsiannikov, V.D. Ultrastable Optical Clock with Neutral Atoms in an Engineered Light Shift Trap. *Phys. Rev. Lett.* **2003**, *91*, 173005. [CrossRef]
5. Haas, M.; Jentschura, U.D.; Keitel, C.H.; Kolachevsky, N.; Herrmann, M.; Fendel, P.; Fischer, M.; Udem, T.; Holzwarth, R.; Hänsch, T.W.; et al. Two-photon excitation dynamics in bound two-body Coulomb systems including AC Stark shift and ionization. *Phys. Rev. A* **2006**, *73*, 052501. [CrossRef]
6. Parthey, C.G.; Matveev, A.; Alnis, J.; Bernhardt, B.; Beyer, A.; Holzwarth, R.; Maistrou, A.; Pohl, R.; Predehl, K.; Udem, T.; et al. Improved Measurement of the Hydrogen 1S–2S Transition Frequency. *Phys. Rev. Lett.* **2011**, *107*, 203001. [CrossRef]
7. Haas, M.; Jentschura, U.D.; Keitel, C.H. Comparison of classical and second quantized description of the dynamic Stark shift. *Am. J. Phys.* **2006**, *74*, 77–81. [CrossRef]
8. Kawasaki, A. Magic wavelength for the hydrogen $1S$–$2S$ transition. *Phys. Rev. A* **2015**, *92*, 042507. [CrossRef]
9. Adhikari, C.M.; Kawasaki, A.; Jentschura, U.D. Magic Wavelength for the hydrogen $1S$–$2S$ transition: Contribution of the continuum and the reduced-mass correction. *Phys. Rev. A* **2016**, *94*, 032510. [CrossRef]

10. Ye, J.; Kimble, H.J.; Katori, H. Quantum State Engineering and Precision Metrology Using State-Insensitive Light Traps. *Science* **2008**, *320*, 1734–1738. [CrossRef]
11. Goldschmidt, E.A.; Norris, D.C.; Koller, S.B.; Wyllie, R.; Brown, R.C.; Porto, J.V.; Safronova, U.I.; Safronova, M.S. Magic wavelengths for the 5*s*–18*s* transition in rubidium. *Phys. Rev. A* **2015**, *91*, 032518. [CrossRef]
12. D. Yin and, Zhang, Y.H.; Li, C.B.; Zhang, X.Z. Magic wavelengths for the 1*S*–2*S* and 1*S*–3*S* transitions in hydrogen atoms. *Chin. Phys. Lett.* **2016**, *33*, 073101. [CrossRef]
13. Jentschura, U.D.; Kotochigova, S.; Le Bigot, E.O.; Mohr, P.J.; Taylor, B.N. Precise Calculation of Transition Frequencies of Hydrogen and Deuterium Based on a Least-Squares Analysis. *Phys. Rev. Lett.* **2005**, *95*, 163003. [CrossRef]
14. For an Interactive Database of Hydrogen and Deuterium Transition Frequencies. Available online: http://physics.nist.gov/hdel (accessed on 10 October 2021).
15. Pachucki, K.; Weitz, M.; Hänsch, T.W. Theory of the hydrogen-deuterium isotope shift. *Phys. Rev. A* **1994**, *49*, 2255–2259. [CrossRef]
16. Pachucki, K.; Leibfried, D.; Weitz, M.; Huber, A.; König, W.; Hänsch, T.W. Theory of the energy levels and precise two-photon spectroscopy of atomic hydrogen and deuterium. *J. Phys. B* **1996**, *29*, 177–195. [CrossRef]
17. Parthey, C.G.; Matveev, A.; Alnis, J.; Pohl, R.; Udem, T.; Jentschura, U.D.; Kolachevsky, N.; Hänsch, T.W. Precision Measurement of the Hydrogen-Deuterium 1*S*–2*S* Isotope Shift. *Phys. Rev. Lett.* **2010**, *104*, 233001. [CrossRef]
18. Gavrila, M.; Costescu, A. Retardation in the Elastic Scattering of Photons by Atomic Hydrogen. *Phys. Rev. A* **1970**, *2*, 1752–1758. Erratum: *Phys. Rev. A* **1971**, *4*, 1688. [CrossRef]
19. Swainson, R.A.; Drake, G.W.F. A unified treatment of the non-relativistic and relativistic hydrogen atom I: The wavefunctions. *J. Phys. A* **1991**, *24*, 79–94. [CrossRef]
20. Swainson, R.A.; Drake, G.W.F. A unified treatment of the non-relativistic and relativistic hydrogen atom II: The Green functions. *J. Phys. A* **1991**, *24*, 95–120. [CrossRef]
21. Swainson, R.A.; Drake, G.W.F. A unified treatment of the non-relativistic and relativistic hydrogen atom III: The reduced Green functions. *J. Phys. A* **1991**, *24*, 1801–1824. [CrossRef]
22. Pachucki, K. Higher-Order Binding Corrections to the Lamb Shift. *Ann. Phys.* **1993**, *226*, 1–87. [CrossRef]
23. Jentschura, U.; Pachucki, K. Higher-order binding corrections to the Lamb shift of 2*P* states. *Phys. Rev. A* **1996**, *54*, 1853–1861. [CrossRef]
24. Jentschura, U.D.; Adhikari, C.M.; Debierre, V. Virtual Resonant Emission and Oscillatory Long–Range Tails in van der Waals Interactions of Excited States: QED Treatment and Applications. *Phys. Rev. Lett.* **2017**, *118*, 123001. [CrossRef] [PubMed]
25. Adhikari, C.M.; Debierre, V.; Matveev, A.; Kolachevsky, N.; Jentschura, U.D. Long-range interactions of hydrogen atoms in excited states. I. 2*S*–1*S* interactions and Dirac–δ perturbations. *Phys. Rev. A* **2017**, *95*, 022703. [CrossRef]
26. Adhikari, C.M.; Debierre, V.; Jentschura, U.D. Adjacency graphs and long-range interactions of atoms in quasi-degenerate states: applied graph theory. *Appl. Phys. B* **2017**, *123*, 1. [CrossRef]
27. Jentschura, U.D.; Debierre, V. Long-range tails in van der Waals interactions of excited-state and ground-state atoms. *Phys. Rev. A* **2017**, *95*, 042506. [CrossRef]
28. Adhikari, C.M. Long-Range Interatomic Interactions: Oscillatory Tails and Hyperfine Perturbations. Ph.D. Thesis, Missouri University of Science and Technology, Rolla, MO, USA, 2017; unpublished.
29. Adhikari, C.M.; Debierre, V.; Jentschura, U.D. Long-range interactions of hydrogen atoms in excited states. III. *nS*–1*S* interactions for $n \geq 3$. *Phys. Rev. A* **2017**, *96*, 032702. [CrossRef]
30. Jentschura, U.D.; Debierre, V.; Adhikari, C.M.; Matveev, A.; Kolachevsky, N. Long-range interactions of excited hydrogen atoms. II. Hyperfine-resolved 2*S*–2*S* system. *Phys. Rev. A* **2017**, *95*, 022704. [CrossRef]
31. Edmonds, A.R. *Angular Momentum in Quantum Mechanics*; Princeton University Press: Princeton, NJ, USA, 1957.
32. Castillejo, L.; Percival, I.C.; Seaton, M.J. On the Theory of Elastic Collisions Between Electrons and Hydrogen Atoms. *Proc. R. Soc. Lond. Ser. A* **1960**, *254*, 259–272.
33. Johnson, W.R.; Blundell, S.A.; Sapirstein, J. Finite basis sets for the Dirac equation constructed from *B* splines. *Phys. Rev. A* **1988**, *37*, 307–315. [CrossRef]
34. Salomonson, S.; Öster, P. Solution of the pair equation using a finite discrete spectrum. *Phys. Rev. A* **1989**, *40*, 5559–5567. [CrossRef] [PubMed]
35. Kramida, A.E. A critical compilation of experimental data on spectral lines and energy levels of hydrogen, deuterium, and tritium. *At. Data Nucl. Data Tables* **2010**, *96*, 586–644. [CrossRef]
36. Anh Thu, L.; Van Hoang, L.; Komarov, L.I.; Romanova, T.S. Relativistic dynamical polarizability of hydrogen-like atoms. *J. Phys. B* **1996**, *91*, 2897–2906.
37. Yakhontov, V. Relativistic Linear Response Wave Functions and Dynamic Scattering Tensor for the $ns_{1/2}$-States in Hydrogenlike Atoms. *Phys. Rev. Lett.* **2003**, *91*, 093001. [CrossRef] [PubMed]
38. Puchalski, M.; Jentschura, U.D.; Mohr, P.J. Blackbody-radiation correction to the polarizability of helium. *Phys. Rev. A* **2011**, *83*, 042508. [CrossRef]